CHAPTER 5

INTERMOLECULAR REACTIVITY OF TETRANUCLEAR FE CLUSTERS VIA PUTATIVE FE–OXO AND –IMIDO INTERMEDIATES

ABSTRACT

Sterically open pyrazolate-bridged tetranuclear Fe clusters were examined for their reactivity towards oxygen and nitrogen transfer reagents. Addition of iodosylarene to a $Fe^{II}_2Fe^{III}_2$ cluster produces a one electron oxidized terminal-hydroxide cluster, which ultimately forms an octanuclear μ_2-O cluster, upon dehydration. Formation of the terminal hydroxide cluster is considered to occur due to formal hydrogen atom abstraction from a reactive intermediate that could not be extensively characterized (either terminal Fe-oxo or iodosylarene adduct). The one electron reduced pyrazolate cluster is capable of activating electron deficient aryl azides, leading to isolation of clusters bearing an NHAr amide ligand, via a putative Fe-imido moiety. Reactivity studies were also performed with an interstitial fluoride containing Fe cluster. Oxygen atom transfer to a μ_4-F containing Fe^{II}_4 cluster leads to formation of analogous octanuclear μ_2-O cluster, or cluster rearrangement to afford a fluoride bound μ_4-O cluster. The intermolecular reactivity of these putative Fe-oxo and –imido moieties were limited to decomposition by formal hydrogen atom transfer in solution, which highlights the high reactivity of these complexes, likely due, in part, to the open coordination environment of the unsubstituted bridging pyrazolates.

INTRODUCTION

Nature utilizes a variety of multinuclear transition metal arrangements to accomplish many catalytic transformations.[1] Three general cases can be considered for the roles these clusters possibly have in metalloenzymes: (i) the transfer of electrons, with no direct substrate-cluster binding or interaction (i.e. [4Fe-4S] clusters); (ii) binding and activation of substrate at a single metal site with the auxiliary metals providing a specific structural or electronic environment for the substrate-binding metal; or (iii) binding and activation of substrate across multiple metal sites within the cluster. Often, the precise role of each metal center within an active site cluster is ambiguous, based on the available biochemical data. Therefore, developing our understanding of the reactivity of transition metal clusters related to these metalloenzymes can help establish the functional purposes of their unique multinuclear architectures.

A number of synthetic mononuclear transition metal complexes have been studied with the goal of providing insight into biological multinuclear active sites that are thought to activate substrates at a single metal site.[2] Due to a number of strategies to tune the reactivity of transition metal complexes through ligand modifications, and the relative ease of structural and spectroscopic characterization of these small molecules, the transition metal chemistry of these systems, which are relevant to biological processes, can be probed in fine detail. However, these studies are not able to establish the possible role of auxiliary metal centers within multinuclear active sites. Examples of multinuclear systems where the reactivity of one metal site can be probed as a function of an auxiliary metal are relatively rare,[3] with most examples limited to binuclear complexes.[4]

A challenge to developing better models of multinuclear active sites, where the level of detail in study can match that of mononuclear systems, lies in the difficulty of producing well-defined multinuclear structures which bear distinct metal coordination environments,

specifically ones where substrate binding and activation is limited to a single metal site within the cluster. These 'site-differentiated' clusters require a fine balance of stability and reactivity to be suitable for detailed studies of their property-reactivity relationships. Along these lines, our group has developed routes to synthesize a family of transition metal clusters supporting various first row transition metal centers (Mn, Fe, Co, Ni, Cu, Zn) in a robust scaffold that arranges the metal in a site-differentiated fashion capable of supporting these property-reactivity studies.[5] These clusters are all based on a common symmetric trinuclear metal precursor, where a fourth (apical) metal site is introduced through the use of bridging pyrazolates (or imidazolates), and anchored into a tetrahedral metal arrangement through a central interstitial μ_4-atom ligand (either O or F).[6] The resulting apical metal center is four coordinate, with a trigonal pyramidal geometry, suitable to study its reactivity as a function of the auxiliary coordinatively saturated metal ions.

The reactivity of these clusters towards accessing M=E (E = O, N) moieties is appealing to study, due to the implication of terminal Mn=O species in the OEC of photosystem II[7] and the possibility of Fe=NR intermediates in nitrogenase FeMo cofactor.[8] Understanding the ways in which neighboring metal centers can affect the nature of these reactive intermediates, therefore, has relevance towards our understanding of multinuclear active sites. Furthermore, interest in the chemistry of these types of reactive intermediates has led to many examples of mononuclear systems capable of supporting these moieties;[9] significantly less developed is the chemistry of these intermediates in complexes with more than two redox active metals.[10]

Previous attempts to examine oxygen- or nitrogen-atom transfer reactivity through terminal M=E intermediates were performed by a number of group members on various pyrazolate-bridged clusters of Fe and Mn. Dr. Graham de Ruiter and Kurtis Carsch studied intramolecular oxygen atom transfer reactions between Fe_4, Mn_4, and Fe_3Mn clusters bearing

arylpyrazolate ligands (Scheme 1);[6b, 11] fast C–H (or C–F) activation of the pendant arene moiety was observed, precluding any reactivity with external substrates, even in large excesses. Attempts to observe intermolecular reactivity led to the development of clusters supported by unsubstituted pyrazolate ligands by Dr. Kyle Horak.[12] Early synthetic routes to these clusters relied on $FeCl_2$ as the source of the apical metal, leading to isolation of **[LFe$_3$O(Pz)$_3$FeCl][OTf]**; removal of the Cl ligand proved challenging, precluding extensive reactivity studies. Exchange of the Cl^- ligand for N_3^- was accomplished, serving as a possible precursor to a reactive Fe-nitride cluster; however, photolysis or thermolysis of this cluster did not lead to activation of the azide ligand.

Scheme 1. Related Studies of Tetranuclear Clusters By Previous Members of the Agapie Group[6b, 11-12]

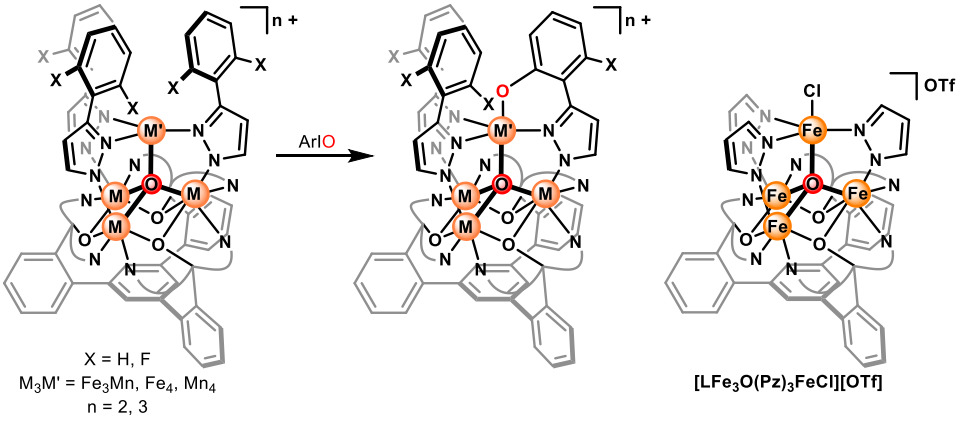

Herein is an extension of the chemistry of the tetranuclear Fe clusters supported by unsubstituted pyrazolate ligands, towards examining intermolecular reactivity via Fe=O or Fe=NR intermediates. Characterization of reaction products demonstrates decomposition by formal hydrogen atom transfer of these putative intermediates to produce the corresponding Fe–OH and Fe–NHR (R = -aryl or –tosyl) species.

RESULTS AND DISCUSSION

Synthesis and Characterization of Fe_4 Clusters Bearing Unsubstituted Pyrazolate Ligands with a Labile Apical Fe Ligand. Tetranuclear Fe clusters with unsubstituted pyrazolates and a labile trifluoromethanesulfonate (triflate, ⁻OTf) ligand bound to the apical Fe can be prepared in two steps starting from the reported tri-iron cluster **$LFe_3(OAc)(OTf)_2$** by stirring this cluster with three equivalents potassium pyrazolate (KPz), iodosylbenzene (PhIO), and Fe(II) acetate (Figure 1A). This produces a tetranuclear Fe cluster bearing unsubstituted pyrazolate ligands and an acetate ligand bound to the apical Fe, **1**. A partial X-ray crystal diffraction dataset was collected to confirm the identity of this cluster; the bond metrics of the Fe–μ_4-O distances were similar to the previously synthesized Fe_4-chloride

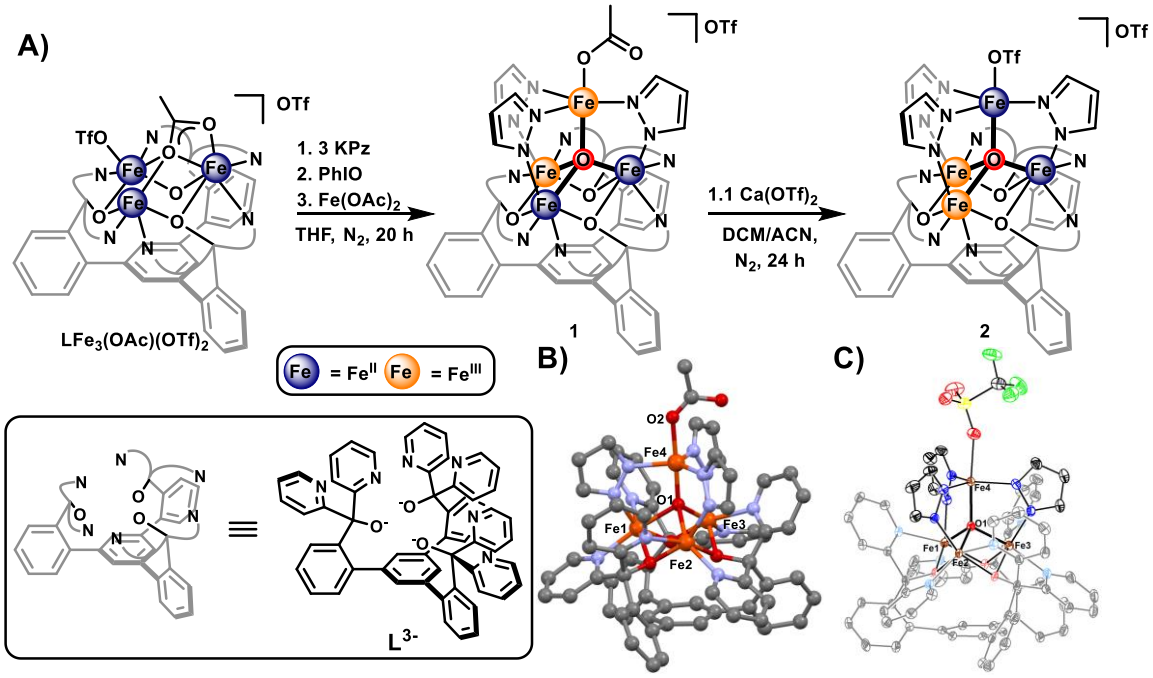

Figure 1. (A) Synthesis of tetranuclear Fe clusters with unsubstituted pyrazolate ligands and labile ligands bound to the apical Fe; inset, 1,3,5-triarylbenzene ligand platform (**L^{3-}**). (B) Preliminary crystal structure of **1** and crystal structure of **2** (C); hydrogen atoms, outersphere anions, and solvent molecules omitted for clarity.

cluster of the same oxidation state, consistent with a redox distribution where the apical Fe is trivalent (Table 1). Addition of calcium triflate to this cluster (to precipitate the less soluble calcium acetate) affords isolation of the tetra-iron dication bis-triflate, **2**. Structural characterization by XRD displays binding of the a triflate counterion to the apical Fe, with changes in the Fe–μ_4-O distances consistent with reduction of the apical Fe to the 2+ oxidation state, and concomitant oxidation of an Fe in the tri-iron core to Fe^{III}. This is supported by the Mössbauer spectrum of **2**, which contains parameters for the apical Fe consistent with a five-coordinate high-spin Fe^{II} (δ = 0.95 mm/s; $|\Delta E_q|$ = 2.22 mm/s; Figure 2 and Table 2).

Table 1. Selected Bond Distances for Structurally Characterized Pz-Fe_4 Clusters

Metric (Å) [b]	$[LFe_3O(Pz)_3Fe(Cl)][OTf]^{12}$	**1**[a]	**3-MeCN**	**2**	**4**
Fe1-O1	2.071(4)	2.17	2.086(9)	2.055(6)	2.143(7)
Fe2-O1	2.145(3)	2.15	2.049(8)	**2.018(5)**	**1.977(7)**
Fe3-O1	**2.024(4)**	**1.91**	**1.926(9)**	**1.949(5)**	**1.989(6)**
Fe4-O1	**1.864(4)**	**1.87**	1.977(8)	1.999(5)	**1.959(6)**
Fe4-L	2.339(2) (Fe4-Cl)	2.04 (Fe4-O2)	2.169(11) (Fe4-N2)	2.155(6) (Fe4-O2)	2.087(8) (Fe4-O2)

[a]Preliminary structure [b]Bold bond distances denote bonds with Fe^{III} centers, the rest are assigned to Fe^{II}.

Cyclic voltammetry of **2** in acetonitrile (MeCN) displays two quasi-reversible peaks, corresponding to the oxidation and reduction of **2**, with reduction potentials of -0.89 V (all potentials vs. Fc/Fc^+) and -0.13 V (Figure 3). A second quasi-reversible oxidation is observed at 0.57 V, however the return reductive scan produces new electrochemical events, suggesting a putative Fe^{III}_4 cluster is accessible, but unstable under the electrochemical conditions. The reduced and oxidized clusters **3** and **4** were accessed through treatment of **2** with cobaltocene ($CoCp_2$) and silver triflate (AgOTf), respectively (Figure 2). Mössbauer spectra of these clusters was consistent with reduction of **2** occurring at an Fe within the tri-iron core, but oxidation

occurring at the apical Fe, as opposed to the Fe^{II} in the core. This is an unusual observation for these types of tetranuclear clusters, where redox changes are typically restricted to the six-coordinate metal centers (only when there are changes to are ligand bound to the apical metal are redox changes for that metal observed). The redox distribution of **4** can be reversibly perturbed by displacement of triflate bound to the apical Fe; the solution state Mossbauer spectrum of **4** in MeCN (**4-MeCN**) displays notable changes to the parameters for the Fe centers, consistent with the loss of high-spin Fe^{II} in the tri-iron core and reduction of the apical Fe.

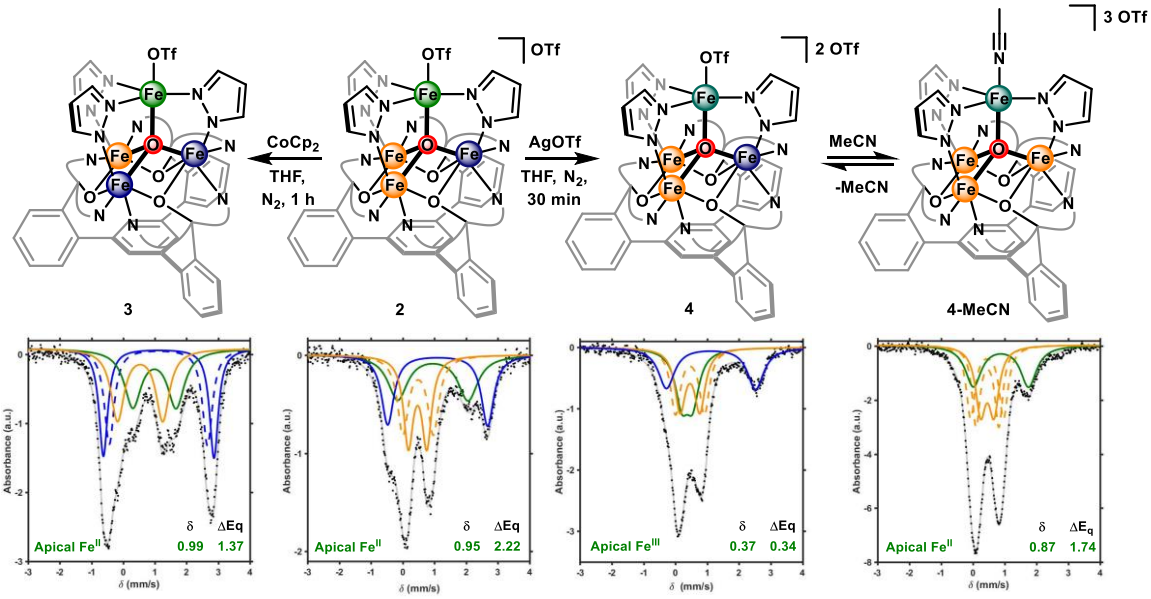

Figure 2. Chemical reduction and oxidation of **2** to afford **3** and **4**, respectively. Zero applied-field ^{57}Fe Mössbauer spectra of these clusters in the solid state, and **4** in a solution of MeCN (**4-MeCN**).

Table 2. ^{57}Fe Mössbauer Parameters for Pz-Fe$_4$ Clusters 2 – 4, and 4-MeCN

	δ (mm/s)	$\|\Delta E_q\|$ (mm/s)	assign-ment
3 ($Fe^{II}_3Fe^{III}$)			
Fe1, Fe2	1.12, 1.11	3.49, 3.10	*h.s.* Fe^{II}
Fe3	0.53	1.43	*h.s.* Fe^{III}
Fe4	0.99	1.37	*h.s.* apical Fe^{II}
2 ($Fe^{II}_2Fe^{III}_2$)			
Fe1	1.10	3.15	*h.s.* Fe^{II}
Fe2, Fe3	0.47, 0.48	0.58, 0.96	*h.s.* Fe^{III}
Fe4	0.95	2.22	*h.s.* apical Fe^{II}

	δ (mm/s)	$\|\Delta E_q\|$ (mm/s)	assign-ment
4 ($Fe^{II}Fe^{III}_3$)			
Fe1	1.12	2.81	*h.s.* Fe^{II}
Fe2, Fe3	0.46, 0.48	0.62, 0.91	*h.s.* Fe^{III}
Fe4	0.37	0.34	*h.s.* apical Fe^{III}
4-MeCN ($Fe^{II}Fe^{III}_3$)			
Fe1, Fe2, Fe3	0.45, 0.46, 0.46	1.03, 0.72, 0.42	*h.s.* Fe^{III}
Fe4	0.89	1.74	*h.s.* apical Fe^{II}

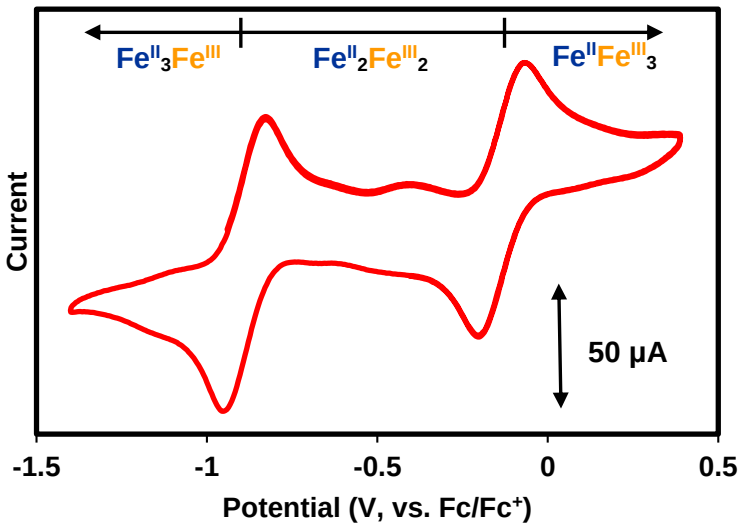

Figure 3. Cyclic voltammetry of **2** in MeCN (2 mM) with $[Bu_4N][PF_6]$ electrolyte (100 mM) at a scan rate of 200 mV/s with glassy carbon, Pt-wire, and Ag-wire as working, counter, and reference electrode, respectively. The open circuit potential was -0.4 V.

Investigations of Pz-Fe$_4$ Clusters with Oxygen Atom Transfer Reagents. With access to these pyrazolate-bridged Fe clusters with a relatively labile ligand (OTf) bound to the site-differentiated Fe, their reactivity towards oxygen atom transfer (OAT) agents were investigated towards performing reactivity studies through a terminal Fe-oxo moiety. Treatment of the [$Fe^{II}_2Fe^{III}_2$] cluster, **2**, with 2-*tert*-butyl-sulfonyl iodosylbenzene (sPhIO) produces a [$Fe^{II}Fe^{III}_3$] cluster with a terminal hydroxide ligand bound to the apical Fe, **5**, based on TOF-MS, ^{1}H NMR spectroscopy, and Mössbauer spectroscopy (Figure 4). This cluster decomposes upon standing, or if concentrated under vacuum, to produce an octanuclear Fe

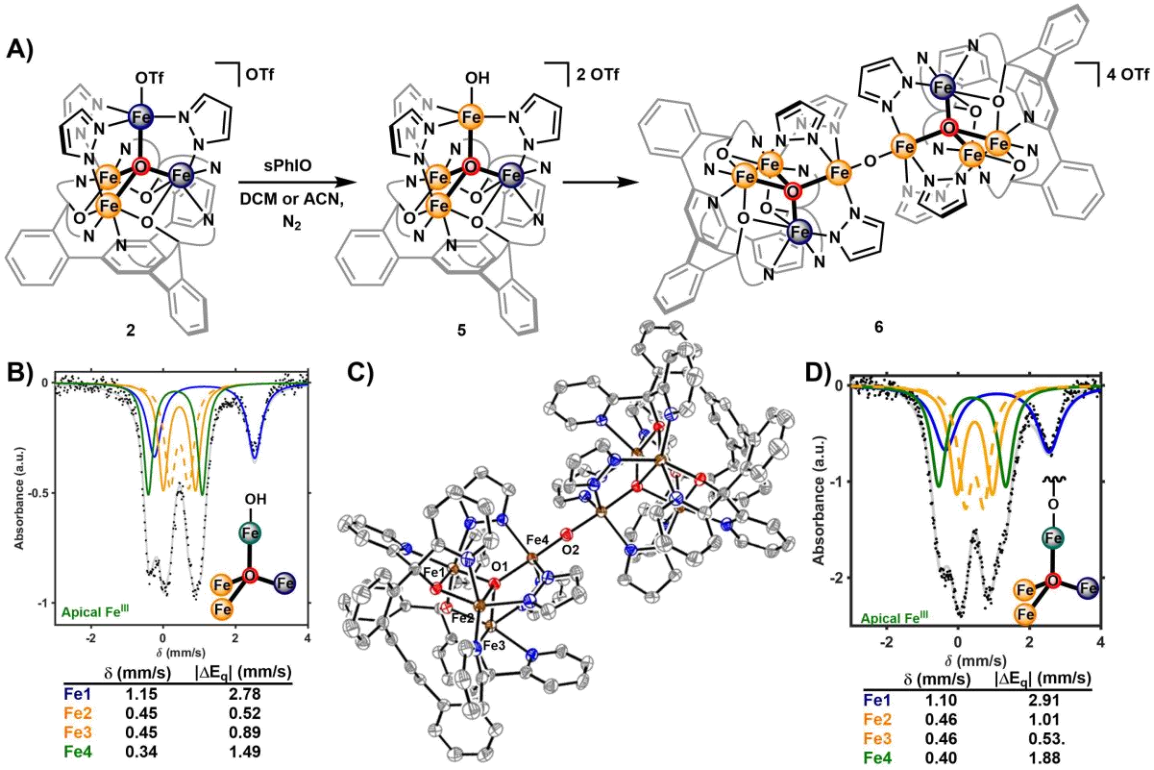

Figure 4. (A) Reactivity of **2** towards OAT reagent sPhIO. (B) Zero applied-field Mössbauer spectrum of **5** in MeCN with parameters for each unique quadrupole doublet. (C) Structure of **6**, with hydrogen atoms, outersphere counterions, and solvent molecules omitted for clarity. (D) Zero applied-field Mössbauer spectrum of **6** in MeCN with parameters for each unique quadrupole doublet.

cluster with a μ_2-O ligand bound to two pyrazolate-bridged [$Fe^{II}Fe^{III}_3$] cluster subunits, **6**; this compound was structurally characterized via XRD. Similar results are obtained with different OAT reagents, such as *tert*-butyl hydroperoxide and tetrabutylammonium *meta*-periodate.

Observation of **5** in solution, likely followed by dehydration to form **6**, supports the conclusion that, under the experimental conditions employed here, a 1:1 cluster to sPhIO stoichiometry is dominant, as opposed to consuming half an equivalent of sPhIO to afford **6** directly. Producing **5** from **2** and sPhIO is consistent with formation of a reactive species which undergoes formal hydrogen atom transfer; both terminal metal-oxo and iodosylarene adduct complexes are known to undergo this type of chemistry.[13]

In an attempt to distinguish between these two possible reactive intermediates, variable temperature ^{1}H NMR experiments were performed. In deuterated solvents (CD_2Cl_2 or CD_3CN) at low temperatures (below -20 °C), mixtures of **5** and a putative intermediate were

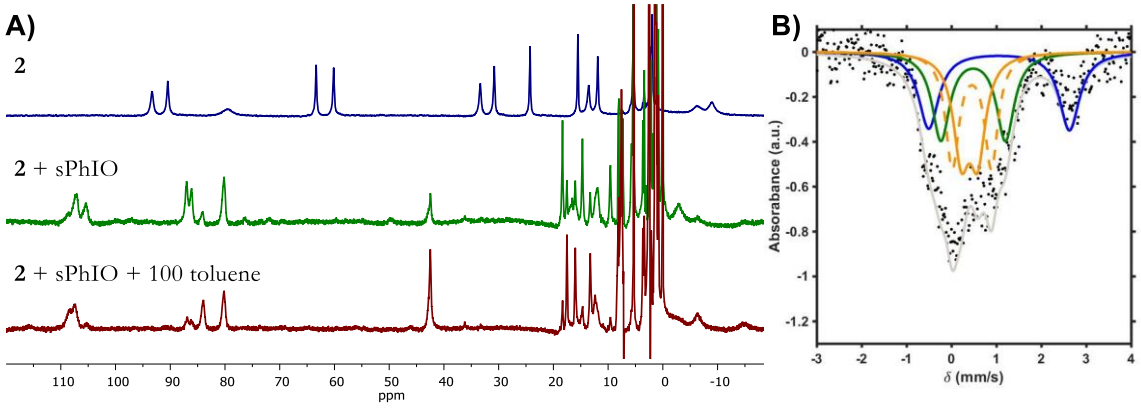

Figure 5. (A) ^{1}H NMR (400 MHz, CD_2Cl_2, -40 °C) spectra of **2** (blue), intermediate of **2** and sPhIO before formation of **5** (green), and **5** formed by addition of excess toluene to this intermediate (red). (B) Mössbauer spectrum of the putative intermediate, collected by cold pentane precipitation, with parameters: (i) δ = 1.06 mm/s, $|\Delta E_q|$ = 3.13 mm/s (blue trace), (ii) δ = 0.40 mm/s, $|\Delta E_q|$ = 0.36 mm/s (solid orange trace), and (iii) δ = 0.46 mm/s, $|\Delta E_q|$ = 0.87 mm/s (dashed orange trace), (iv) δ = 0.49 mm/s, $|\Delta E_q|$ = 1.44 mm/s (green trace).

observed (Figure 5). A Mössbauer spectrum of this mixture was obtained, and it ruled out the presence of an Fe^{IV}-oxo moiety, with parameters that were best fit with **5** and another [$Fe^{II}Fe^{III}_3$] cluster. However, assigning this species to either possible oxidizing intermediate (Fe^{III}-oxo or -iodosylarene adduct) was inconclusive. Analogous experiments were performed on the other oxidation states of the Pz-Fe_4 clusters, **3** and **4**. In neither case could a reactive intermediate be observed by NMR at an appreciable concentration; **3** would react completely, even at -40 °C, while **4** would remain mostly unreacted towards sPhIO at low temperatures.

The electrochemical and spectroscopic properties of **6** were investigated; however, it was later determined that isolation and recrystallization of samples of **6** contained two species by ^{1}H NMR with nearly identical resonances (Figure 6). These species could be separated from each other through extraction of **6** (as confirmed by XRD) in MeCN. Attempts to structurally characterize the remaining MeCN precipitate were unsuccessful.

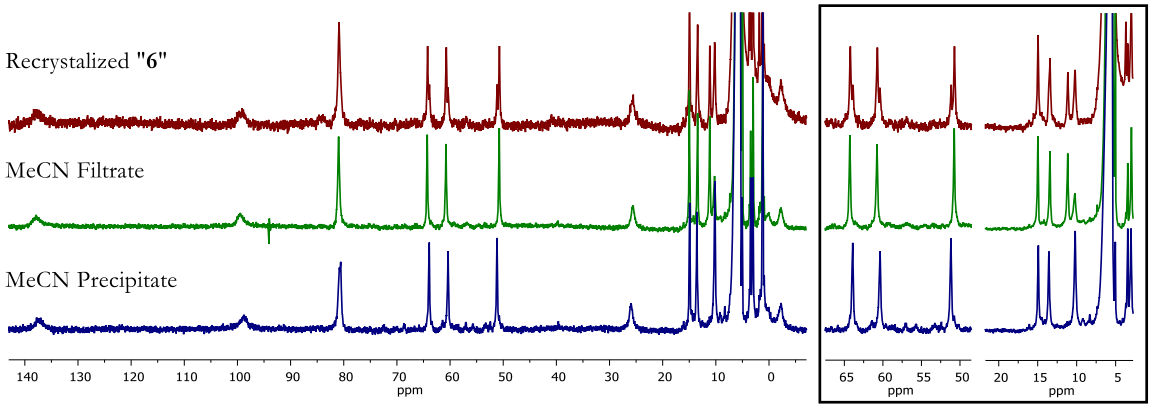

Figure 6. ^{1}H NMR (300 MHz, CD_2Cl_2) of as-isolated and recrystallized **6** (red) and the species separated by trituration in MeCN (green and blue). (Inset) Paramagnetic regions highlighting the differences in peak positions of these two species.

Cyclic voltammetry of **6** in CH_2Cl_2 displays five quasi-reversible redox events separated into closely spaced pairs, attributable to redox changes occurring within each of the tetra-iron

subunits (Figure 7). The reduction potentials of these processes, where the charge of the cluster is used to abbreviate oxidation state (0 = $[Fe^{II}_3Fe^{III}]_2O$, 1+ = $[Fe^{II}_3Fe^{III}]O[Fe^{III}_2Fe^{II}_2]$, etc.): 0 → 1+, -1.98 V (all potentials vs Fc/Fc^+); 1+ → 2+, -1.64 V; 2+ → 3+, -0.75 V; 3+ → 4+, -0.56 V; 4+ → 5+, 0.10 V. The small separation between the pairs of redox events is consistent with relatively little electronic interaction between the individual Pz-Fe_4 subunits. The redox event to form the 6+ cluster ($[Fe^{III}_4]_2O$) was not observed in the CV, or via square-wave voltammetry.

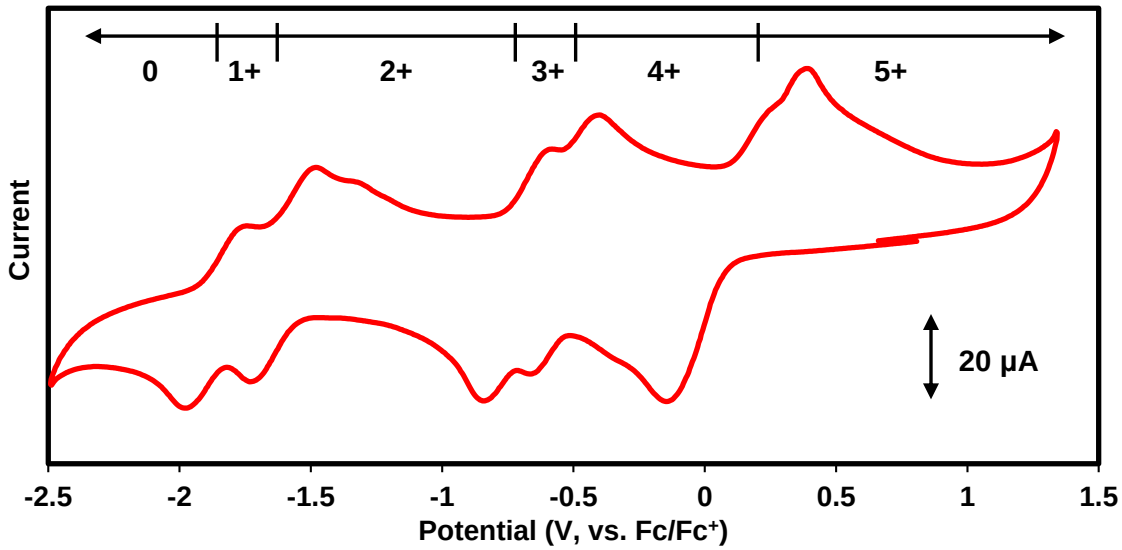

Figure 7. Cyclic voltammetry of **6** in CH_2Cl_2 (2 mM) with $[Bu_4N][PF_6]$ electrolyte (100 mM) at a scan rate of 200 mV/s with glassy carbon, Pt-wire, and Ag-wire as working, counter, and reference electrode, respectively. The open circuit potential was 0 V.

Reactivity of Pz-Fe_4 Clusters with Organic Azides and *N*-Tosylimino-Transfer Reagent. Due to the challenges in observing evidence for formation of, and reactivity from, a terminal Fe-oxo with **2** and OAT reagents, reactions targeting an Fe-imido species were attempted; it was hypothesized that substituents on the nitrogen atom could be selected to stabilize the Fe-bound intermediate, i.e. having a bulky, electron withdrawing group would

slow down decomposition by formal hydrogen atom transfer, and disfavor formation of μ_2-NR clusters (analogous to **6**). **2** proved to be unreactive towards aryl- or alkyl-azides, but the one electron reduced cluster, **3**, was competent for activation of relatively electron poor aryl azides. These reactions were typically complete upon warming to room temperature; preliminary structural characterization of reactions between **3** and 2-azideobiphenyl and 3,5-trifluoromethyl-phenylazide displayed apical Fe centers with a coordinated aryl amide (–NHAr), as evidenced by the relatively long apical Fe–N distance of ~2.0 Å and small Fe–N–C angle of ~130°, consistent with reported structures of Fe^{III}–NHAr complexes.[14]

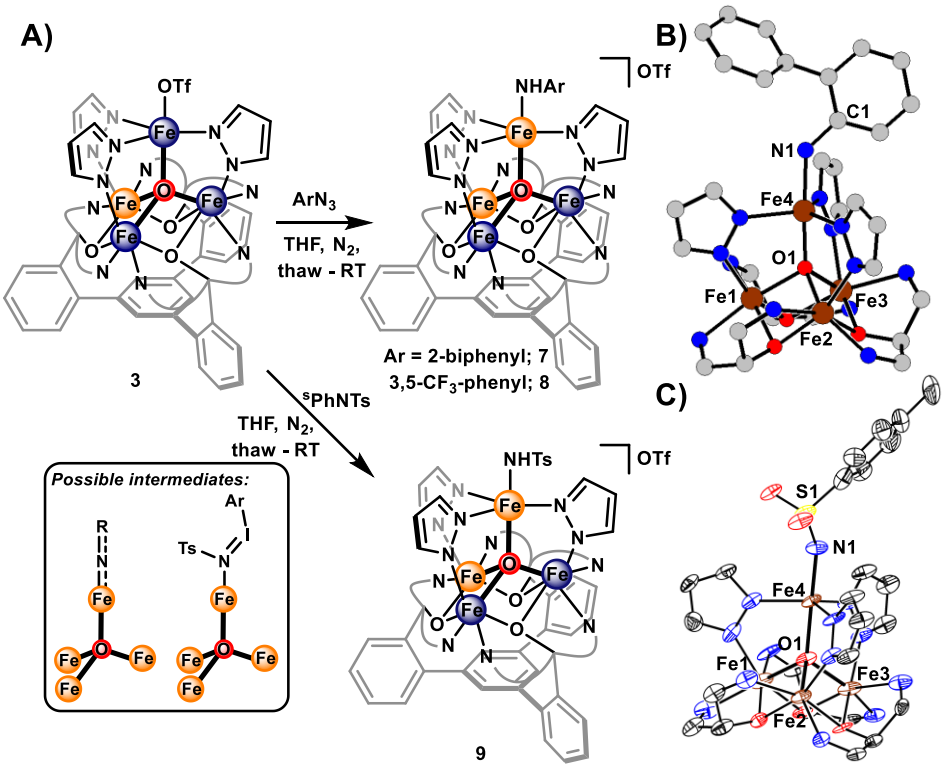

Figure 8. (A) Synthesis of aryl- and tosyl-amide clusters **7** – **9** from **3**; (inset) possible Fe-bound intermediates include a terminal Fe-imido or iodo-tosylimino adduct. (B) Truncated preliminary crystal structure of **7**. (C) Truncated crystal structure of **8**; hydrogen atoms, counterions, and solvent molecules omitted for clarity.

Table 3. Selected Bond Distances and Angles for Complexes 7 – 9.

Metric (Å)[b]	**7**[a]	**8**[a]	**9**
Fe1-O1	2.10	2.16	2.047(8)
Fe2-O1	2.08	2.09	2.044(9)
Fe3-O1	**2.04**	**1.99**	**1.993(7)**
Fe4-O1	**1.87**	**1.90**	**2.035(8)**
Fe4-N1	2.01	1.99	1.856(10)
∠Fe4–N1–C1	131	131	146.8 (∠Fe4–N1–S1)

[a] Preliminary structure. [b]Bold bond distances denote bonds with Fe^{III} centers, the rest are assigned to Fe^{II}.

Similarly, treatment of **3** with an iodoimino transfer agent, 2-*tert*-butyl-sulfonyl-*N*-para-toluenesulfonyl-iminoiodobenzene (sPhNTs), leads to isolation of the tosylamide-bound cluster, **9**.

Overall, attempts to stabilize Fe-imido clusters with electron withdrawing or sterically bulky aryl groups were unable to lead to observation of this intermediate before formal hydrogen atom transfer to produce the corresponding amide. For reactions with aryl azides, it is possible that azide activation leads to a short-lived aryl-imido cluster, although off-metal reactive species cannot be ruled out, i.e. outersphere electron transfer producing reactive nitrene. Application of these reactions towards amination of cyclohexene were attempted, however no N-transfer product was observed.

Reactivity of μ_4-F Pz-Fe_4 Clusters Towards Oxygen Atom Transfer Reagents and Azide. Due to the challenge of observing evidence of a terminal Fe-oxo or –imido moiety within these clusters, investigations on related clusters bearing a different electronic environment were pursued. Previous investigations on μ_4-F bridged clusters demonstrated a significant effect the interstitial ligand has on the properties and reactivity of the Fe_4 cluster (see Chapter 2).[6d] A μ_4-F ligand could make the apical Fe more electron deficient, and any resulting terminal Fe-oxo less basic; furthermore, weaker the bonding to the μ_4-F may promote

multiple bonding to a terminal-oxo by facilitating pseudo-tetrahedral geometry at the apical Fe.

Unsubstituted pyrazolate-bridged clusters bearing an interstitial F^- ligand were prepared through addition of tetrabutylammonium fluoride to **$LFe_3(OAc)(OTf)_2$** with a combination of potassium pyrazolate and two equivalents of pyrazole (HPz). The apical Fe is introduced with $Fe(N(SiMe_3)_2)_2$ and calcium triflate was added to sequester acetate from the initial trinuclear cluster, to afford isolation of a fluoride-bridged Fe^{II}_4 cluster, **10** (Scheme 2).

Scheme 2. Synthesis and Reactivity of Pz-Fe_4 Clusters Bearing μ_4-F Ligand.

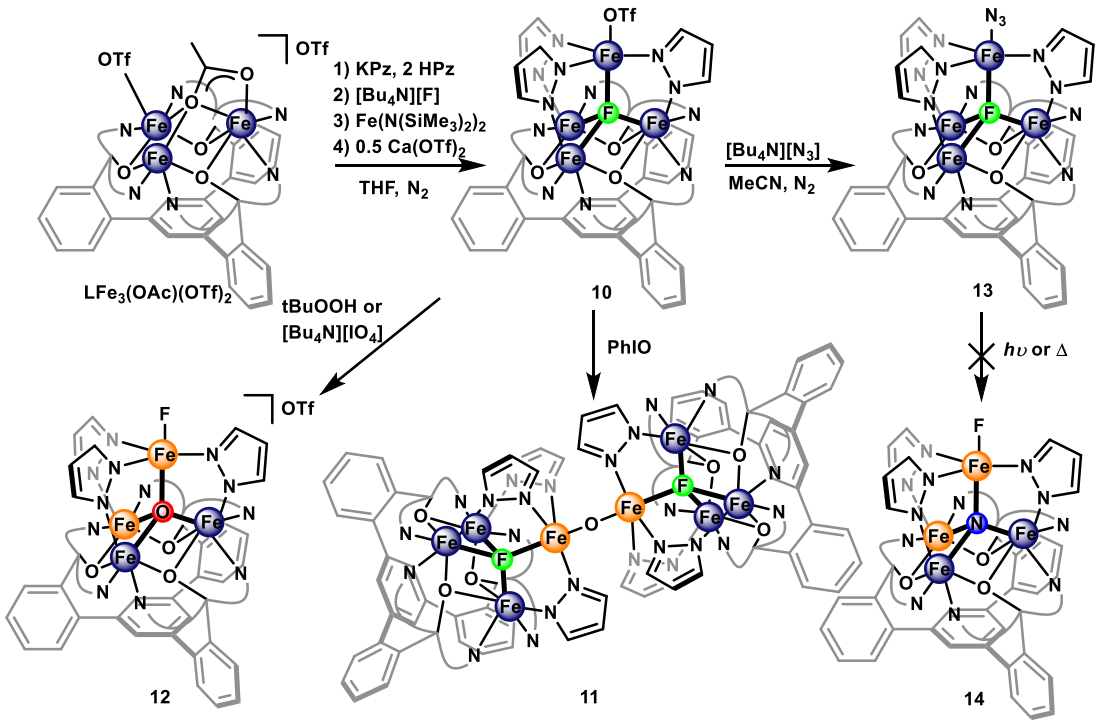

Structural characterization of **10** confirms a cluster geometry analogous to the μ_4-O versions (Figure 9A). The electrochemistry of this cluster is more complex than **2**. In MeCN, only one quasi-reversible feature is observed, corresponding to a reduction potential for the oxidation of **10** at -0.52 V (vs. Fc/Fc^+), followed by two irreversible oxidations, which change

over multiple CV scans (Figure 10), likely due to decomposition of the $Fe^{II}Fe^{III}_3$ cluster oxidation state.

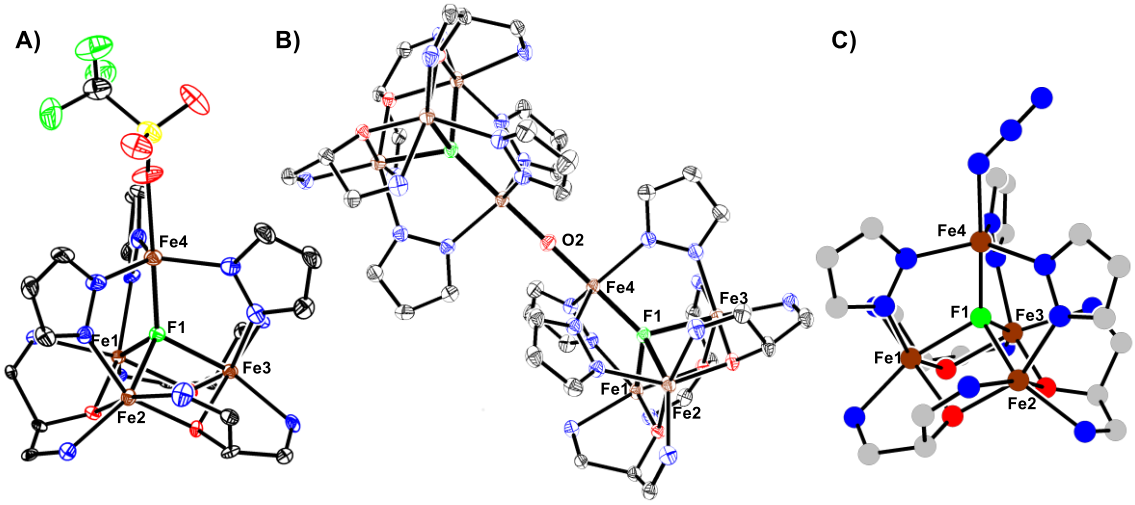

Figure 9. Truncated crystal structures of **10** (A), **11** (B), and **13** (C; preliminary).

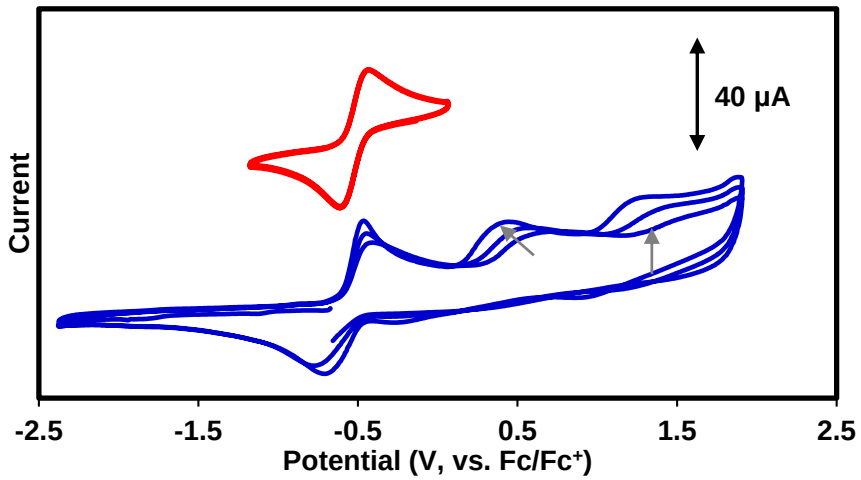

Figure 10. Cyclic voltammetry of **10** in MeCN (2 mM) with $[Bu_4N][PF_6]$ electrolyte (100 mM) at a scan rate of 200 mV/s with glassy carbon, Pt-wire, and Ag-wire as working, counter, and reference electrode, respectively. The open circuit potential was -0.7 V. The full CV scan (blue) displays two irreversible oxidations, which shift over multiple CV scans.

Treatment of **10** with different OAT reagents results in multiple reaction products, with product distributions that depends on the nature of the OAT reagent. Reactions with

iodosylbenzene (PhIO), which is polymeric and insoluble, leads to isolation of a μ_2-O cluster (**11**), with a structure analogous to **6** (Figure 9B). Analysis of bond metrics of **6** and **11** display shorter bonds to the μ_2-O in **11** (1.7853(6) vs. 1.8079(7) Å), with a shift of the apical Fe out of the equatorial plane (Table 4).

Table 4. Selected Bond Distances in Complexes 6 and 11.

Metric (Å)	**6** ($[Fe^{II}Fe^{III}_3]_2O$)	**11** ($[Fe^{II}_3Fe^{III}]_2O$)
Fe1-O1/F1	**1.942(3)**	2.191(2)
Fe2-O1/F1	**2.096(3)**	2.205(2)
Fe3-O1/F1	2.176(3)	2.235(2)
Fe4-O1/F1	**1.925(3)**	**1.991(2)**
Fe4-O2	1.8079(7)	1.7853(6)
Fe4-N14|N24|N34	0.099	0.174

Alternatively, *tert*-butyl hydroperoxide (tBuOOH) or tetrabutylammonium periodate ($[Bu_4N][IO_4]$) react very quickly with **10** to produce a species which is assigned to an interstitial O cluster with a terminal F ligand, **12**. This is supported by independent synthesis of **12** from **1** and tetrabutylammonium fluoride, as evidenced by ^{1}H NMR spectroscopy. A possible intermediate to **12** could be a terminal Fe-oxo, followed by internal ligand rearrangement to form the more stable interstitial oxo cluster, although direct substitution of the μ_4-F by the OAT reagent is also a possible route to this complex.

Observation of substitution of the μ_4-F in **10** suggested a potential route to tetranuclear clusters with a bridging nitride ligand, via formation of a terminal nitride that undergoes cluster rearrangement. The azide-bound Pz-Fe_4 cluster, **13**, can be prepared through addition of tetrabutylammonium azide to **10** (Figure 9C). Attempts to thermalyze or photolyze this moiety, however, led to no reaction being observed (Scheme 1).

CONCLUSIONS

A series of tetranuclear Fe clusters bearing a sterically open coordination environment at the apical Fe could be prepared with a coordinated labile triflate ligand, suitable for reactivity studies towards oxygen and nitrogen atom transfer reagents. For **2**, and its one electron reduced form, **3**, fast intermolecular decomposition of putative Fe-oxo and Fe-imido moieties (or iodosylarene adducts) occur by formal hydrogen atom transfer, likely from organic solvent. A cluster bearing an interstitial F ligand, **10**, demonstrated similar reactivity, forming an octanuclear μ_2-O cluster containing fluoride, but was also capable undergoing substitution of this interstitial fluoride ligand with oxygen.

Overall, it is challenging to reach a suitable balance between stability and reactivity for these Pz-Fe_4 clusters to prepare terminal-oxo or -imido moieties. Subsequent studies demonstrated the necessity of pendant hydrogen bonding donors on the pyrazolate ligands to stabilize an Fe-oxo (Chapter 4). Further investigations could examine strategies to tune these secondary coordination sphere interactions to access a suitably reactive, but still well-defined, Fe-oxo cluster.

EXPERIMENTAL DETAILS

General Considerations. All reactions were performed at room temperature in an N_2-filled M. Braun glovebox or using standard Schlenk techniques unless otherwise specified. Glassware was oven dried at 140 ºC for at least 2 h prior to use, and allowed to cool under vacuum. **$LFe_3(OAc)(OTf)_2$**,[6a] potassium pyrazolate (KPz),[6e] iodosobenzene (PhIO),[15], tetrabutylammonium fluoride ($[Bu_4N][F]$),[16], iron(II) bis-hexamethyldisilylamide ($Fe(N(SiMe_3)_2)_2$),[17] 2-*tert*-butyl-sulfonyl-iodosylbenzene (sPhIO),[18] 2-*tert*-butyl-sulfonyl-*N*-para-toluenesulfonyl-iminoiodobenzene (sPhINTs),[18] and 3.5-trifluoromethyl-phenylazide,[19] were prepared according to literature procedures. All organic solvents were dried by sparging with nitrogen for at least 15 minutes, then passing through a column of activated A2 alumina under positive N_2 pressure. ^1H spectra were recorded on a Varian 300 MHz spectrometer; variable temperature spectra were recorded on a Varian 400 MHz spectrometer. CD_3CN and CD_2Cl_2 were purchased from Cambridge Isotope Laboratories, dried over calcium hydride, degassed by three freeze-pump-thaw cycles, and vacuum transferred prior to use.

Physical Methods. *Mössbauer measurements.* Zero field ^{57}Fe Mossbauer spectra were recorded at 80 K in constant acceleration mode on a spectrometer from See Co (Edina, MN) equipped with an SVT-400 cryostat (Janis, Wilmington, WA). The isomer shifts are relative to the centroid of an α-Fe foil signal at room temperature. Samples were prepared by mixing polycrystalline material (20 mg) with boron nitride in a cup fitted with screw cap or freezing a concentrated solution in MeCN. The data were fit to Lorentzian lineshapes using WMOSS (www.wmoss.org).

Mössbauer simulation details for all compounds. All spectra were simulated as four pairs of symmetric quadrupole doubles with equal populations and Lorentzian lineshipes. They were refined to a minimum via least squares optimization (13 fitting parameters per spectrum).

Signals appearing above 2 mm/s were indicative with the presence of high-spin Fe^{II} centers and correspond to species with isomer shifts ~ 1 mm/s. The Mössbauer data were fit to be consistent with our previously reported iron clusters.[6a, 11b, 20] The observed Mossbauer parameters are in agreement with related six-coordinate high-spin Fe^{II}/Fe^{III} centers.[21]

Electrochemical measurements. CVs and SWVs were recorded with a Pine Instrument Company AFCBP1 biopotentiostat with the AfterMath software package. All measurements were performed in a three electrode cell, which consisted of glassy carbon (working; ø = 3.0 mm), silver wire (reference) and bare platinum wire (counter), in a N_2 filled M. Braun glovebox at RT. The ferrocene/ferrocinium (Fc/Fc^+) redox wave were used as an internal standard for all measurements.

X-ray crystallography. X-ray diffraction data was collected at 100 K on a Bruker PHOTON100 CMOS based diffractometer (microfocus sealed X-ray tube, Mo Kα (λ) = 0.71073 Å or Cu Kα (λ) = 1.54178 Å). All manipulations, including data collection, integration, and scaling, were carried out using the Bruker APEXII software. Absorption corrections were applied using SADABS. Structures were solved by direct methods using XS (incorporated into SHELXTL) and refined by using ShelXL least squares on Olex2-1.2.7 to convergence. All non-hydrogen atoms were refined using anisotropic displacement parameters. Hydrogen atoms were placed in idealized positions and were refined using a riding model. Due to the size of the compounds most crystals included solvent-accessible voids that contained disordered solvent. In most cases the solvent could be modeled satisfactorily.

Synthetic Procedures. *Synthesis of [LFe₃O(Pz)₃Fe(OAc)][OTf]* ***(1).*** 627 mg (0.45 mmol) **$LFe_3(OAc)(OTf)_2$** was suspended in 8 mL THF in a 20 mL scintillation vial. This suspension was frozen in a liquid N_2-cooled cold-well. In a separate vial, a suspension of 152 mg (1.43 mmol) potassium pyrazolate in 2 mL was also frozen. The suspensions were combined, while

thawing, and stirred for 10 minutes. Then, 2 mL THF was used to transfer 101 mg (0.46 mmol) iodosylbenzene to the stirring suspension; after 60 minutes, a brown suspension forms. 80 mg (0.465 mmol) $Fe(OAc)_2$ was added to the reaction with 3 mL THF and stirred for 20 hours. The precipitate was collected over a bed of celite on a glass frit, washed with 3 mL THF, and dried under vacuum. A brown solution was collected by washing this solid with CH_2Cl_2 and filtering it through the frit. Recrystallization via CH_2Cl2/Et_2O vapor diffusion affords 375 mg (55% yield) **1** as brown crystals. ^{1}H NMR (300 MHz, CD_2Cl_2) δ 131.9 (br), 83.9 (br), 75.9, 56.6, 50.9, 37.6, 26.2, 22.9, 14.4, 13.6, 11.0, 2.6), 1.3, -2.3 (br), -12.3, -17.8 (br) ppm.

Synthesis of $[LFe_3O(Pz)_3Fe][OTf]_2$ ***(2).*** 124 mg $Ca(OTf)_2$ (0.37 mmol) was dissolved in 10 mL MeCN and 290 mg (0.19 mmol) **1** was added as a 10 mL DCM solution. This was stirred for 24 – 48 hours, until the ^{1}H NMR showed complete conversion to $[LFe_3O(Pz)_3Fe][OTf]_2$. The reaction was dried completely under vacuum, and a green-brown compound was dissolved in 15 mL DCM, filtered over celite, and recrystallized via vapor diffusion of Et_2O. 293 mg (0.184 mmol; 96% yield) of **2** were obtained after drying the resulting crystals under vacuum. X-ray quality crystals were obtained by oxidizing **3** with 1 equivalent $AgBPh_4$ in THF. Crystallization via diffusion of pentane into a CH_2Cl_2 solution of this compound affords crystals of $[LFe_3O(Pz)_3Fe][OTf][BPh_4]$ (^{1}H NMR identical to $[LFe_3O(Pz)_3Fe][OTf]_2$). ^{1}H NMR (300 MHz, CD_3CN) δ 122.0 (br), 71.1, 69.0, 53.3, 50.9, 42.4, 38.4, 16.7, 14.2, 13.9 (br), 12.5, 8.4 (br), 7.2, 3.9, 3.4, -5.5 (br) ppm. ^{19}F NMR (300 MHz, CD_3CN) δ -76 ppm. UV-Vis (CH_3CN) [ε (M^{-1} cm^{-1})]: 246 nm (6.4 x 10^4), 369 nm (6.7 x 10^3). Anal. Calcd. (%) for $C_{68}H_{48}F_6Fe_4N_{12}O_{10}S_2$: C, 51.77; H, 3.03; N, 10.54. Found: C, 51.17; H, 3.11; N, 10.46.

*Synthesis of $[LFe_3O(Pz)_3Fe][OTf]$ (**3**).* A suspension of $[LFe_3O(Pz)_3Fe][OTf]_2$ (**2**; 43.8 mg, 0.027 mmol) in 2 mL THF was stirred as a THF solution of 5.9 mg $CoCp_2$ (0.031 mmol) was added. After 1 hour, the reaction was dried under vacuum. 4 mL DME was added to the purple

solid and stirred for 12 hours. The resulting purple precipitate was collected on a bed of celite, washed with 2 mL DME, dried, and eluted with 2:1 THF/MeCN; crystals of $[LFe_3O(Pz)_3Fe][OTf]$ (**3**) were obtained by vapor diffusion of Et_2O into this solution. ^1H NMR (300 MHz, CD_3CN): 101.8 (br), 59.4, 57.4, 35.8, 30.0, 29.5, 19.5, 15.9, 13.3, 7.2, 4.5, 3.9, -1.6 (br), -5.9 (br) ppm.

*Synthesis of $[LFe_3O(Pz)_3Fe][OTf]_3$ (**4**).* 45 mg (0.03 mmol) of $[LFe_3O(Pz)_3Fe][OTf]_2$ (**2**) was stirred as a suspension in THF. A THF solution of AgOTf (7 mg; 0.03 mmol) was added. After 30 minutes the reaction was dried under vacuum. The resulting solid was filtered over celite with DCM and the filtrate was dried under vacuum. This brown solid was crystallized via vapor diffusion of Et_2O into a DCM/MeCN solution to obtain 47 mg $[LFe_3O(Pz)_3Fe][OTf]_3$ (95% yield). ^1H NMR (300 MHz, CD_3CN) δ 169.0 (br), 94.7 (br), 81.8, 78.9, 72.9, 64.5, 45.0, 17.3, 10.4, 8.5, 7.9, 5.2, -0.8 (br) ppm. ^{19}F NMR (300 MHz, CD_3CN) δ -76 ppm.

*Synthesis of $[LFe_3O(Pz)_3Fe(OH)][OTf]_2$ (**5**). Method A.* 10.8 mg (0.007 mmol) **1** was layered in an NMR tube in MeCN with 100 μL of a 0.11 M MeCN solution of tBuOOH (0.011 mmol; prepared by diluting a 3.3 M stock in toluene) in a liquid N_2-cooled cold well. The layers were mixed upon thawing. **5** decomposes upon pumping down, or standing for long periods of time. In some experiments, excess (~2 equiv.) DABCO was added, but this had no noticeable effect on the production **5**. ^1H NMR (300 MHz, CD_3CN) δ 145.0 (br), 103.7 (br), 85.6, 66.6, 63.9, 45.5, 30.0 (br), 15.3, 13.6, 11.1, 7.2, -3.0 (br) ppm.

Method B. 54 mg (0.034 mmol) **2** was dissolved in 10 mL MeCN and froze in a liquid N_2-cooled cold well. This was combined with 12 mg (0.035 mmol) sPhIO upon thawing and mixed for 30 minutes. This produces an NMR identical to Method A, with a minor amount of **6**, due to decomposition.

*Synthesis of [(LFe$_3$O(Pz)$_3$Fe)$_2$O][OTf]$_4$ (**6**) Method A.* Concentration of a solution of **5** under vacuum produces a change in the NMR consistent with formation of **6**. ^{1}H NMR (300 MHz, CD_2Cl_2) δ 137.4 (br), 98.9 (br), 80.3, 63.7, 60.2, 50.3, 25.3 (br), 14.6, 13.1, 10.8, 9.9, 2.7, 1.7, -2.6 (br) ppm.

Method B. A MeCN solution of **2** was mixed with 0.6 equivalents PhIO for 5 hours at room temperature. The reaction was dried under vacuum and filtered with CH_2Cl_2. This crude product was recrystallized via CH_2Cl2/Et_2O vapor diffusion to obtain mostly **6** (with an unidentified impurity, vide infra), with an NMR identical to Method A.

Regardless of preparation method, a side product (ca. 30% relative to **6**) would be present with nearly identical NMR shifts: ^{1}H NMR (300 MHz, CD_2Cl_2) δ 137.5 (br), 98.7 (br), 80.6, 63.6, 60.1, 50.9, 25.7 (br), 14.6, 13.2, 9.9, 2.7, 0.84, -2.6 (br) ppm. This could be separated from **6** by stirring a solution of the mixture for 18 hours in MeCN and collecting the filtrate, or via MeCN/Et_2O vapor diffusion, where the mother liquor is collected upon precipitation of the side product. Attempts to identify this side product by XRD were unsuccessful.

*Synthesis of [LFe$_3$O(Pz)$_3$Fe(2-phenyl-anilide)][OTf] (**7**).* 22.3 mg (0.014 mmol) **2** was combined with 2.6 mg (0.013 mmol) 2-azidobiphenyl in thawing THF. After 24 hours, no reaction had been observed and 3.8 mg (0.02 mmol) $CoCp_2$ was added to the reaction; the solution turned purple, signifying the formation of **3**, and over multiple hours became blue. After stirring 20 hours, the reaction was recrystallized via THF/pentane vapor diffusion to afford crystals of **7**. ^{1}H NMR (500 MHz, THF/C_6D_6) δ 122.2 (br), 78.5 (br), 71.7, 71.1, 53.2, 47.5, 37.7, 33.4, 21.2, 14.0, 13.5, 11.4, 9.4, -16.8 ppm.

*Synthesis of [LFe$_3$O(Pz)$_3$Fe(3,5-trifluoromethyl-anilide)][OTf] (**8**).* 11.2 mg (0.008 mmol) **3** was dissolved in 3 mL THF and froze in a liquid N_2-cooled cold well. This was combined with a 1 mL solution of 2 mg (0.008 mmol) 3,5-trifluoromethyl phenylazide in THF, while thawing.

The solution turned blue as it warmed to room temperature, producing a mixture of **8** and side products. This was recrystallized via THF/pentane vapor diffusion. ^{1}H NMR (500 MHz, THF/C_6D_6) δ 123.4 (br), 78.9 (br), 70.4, 69.5, 50.7, 44.8, 25.7, 17.1, 8.9, 8.5, -6.8, -25.3 (br) ppm.

*Synthesis of [LFe$_3$O(Pz)$_3$Fe(p-toluenesulfonimide)][OTf] (**9**).* 11.3 mg (0.008 mmol) **3** was dissolved in THF and froze in a liquid N_2-cooled cold well. This was combined with 4.5 mg (0.009 mmol) sPhINTs in THF while thawing. The solution turns orange-red upon warming to room temperature to produce **9**. This was recrystallized via MeCN/Et_2O. ^{1}H NMR (300 MHz, CD_3CN) δ 125.7 (br), 91.6 (br), 73.7, 58.0, 55.1, 51.1, 14.0, 13.4, 534, 3.4, -1.1 (br) ppm.

*Synthesis of [LFe$_3$F(Pz)$_3$Fe][OTf] (**10**).* 763 mg (0.55 mmol) **LFe$_3$(OAc)(OTf)$_2$** was suspended in 5 mL THF in a 20 mL scintillation vial. This suspension was frozen in a liquid N_2-cooled cold-well. In a separate vial, a suspension of 64 mg (0.60 mmol) potassium pyrazolate and 88 mg (1.30 mmol) pyrazole in 2 mL THF was also frozen. These were combined while thawing, followed by addition of a THF suspension of [Bu_4N][F], 156 mg (0.60 mmol). After stirring for 30 minutes, a solution of 210 mg (0.56 mmol) Fe(N($SiMe_3$)$_2$)$_2$ was added. The solvent was removed under vacuum upon stirring for 20 hours. The solid was washed with Et_2O and toluene on a course porosity glass frit with celite; The remaining precipitate was eluted with a 1:1 mixture of THF/MeCN, until the washings from the frit were colorless. The filtrate was dried completely under vacuum, then suspended in 10 mL MeCN. 120 mg (0.34 mmol) Ca(OTf)$_2$ was added to the suspension and stirred for 24 hours. The red orange precipitate was collected over celite, dried under vacuum, then eluted with CH_2Cl_2 and recrystallized via CH_2Cl_2/Et_2O vapor diffusion to yield 450 mg of **10** as red-orange crystals (56% yield). ^{1}H NMR (300 MHz, CD_2Cl_2) δ 110.3 (br), 77.2, 72.5, 40.4, 30.0, 27.1, 23.3, 16.7, 11.9, 11.4, 4.5, 4.1, 1.2, -1.3 (br), -30.1 (br) ppm

*Synthesis of [(LFe$_3$F(Pz)$_3$Fe)$_2$O][OTf]$_2$ (**11**). Method A.* 102 mg (0.07 mmol) **10** was dissolved in CH_2Cl_2 a connected to the Schlenk line in a Schlenk tube. The reaction was degassed with three freeze-pump-thaw cycles and froze with liquid N_2. On the Schlenk line, 10.5 cmHg of O_2 was collected in a volumetric gas bulb (36.7 mL; 0.21 mmol O_2), which was connected between the Schlenk line and the reaction vessel. This was introduced to the frozen solution for 5 minutes, then thawed -78 °C and stirred briefly before warming to -30 °C. The reaction was left open to the partial atmosphere of O_2 for 30 minutes and stirred. Then, the solvent was removed under vacuum and the solid was recrystallized via CH_2Cl_2/Et_2O vapor diffusion to afford crude **11** (with an unidentified side product, vide infra). ^{1}H NMR (300 MHz, CD_2Cl_2) δ 92.1 (br), 77.3, 76.3, 43.2, 42.7 (br), 38.3, 26.7, 25.2, 24.3, 22.1,16.0, 9.2, 0.9, -1.1, -10.5 (br), -11.9 (br) ppm

Method B. 48 mg (0.033 mmol) **10** was dissolved in MeCN and combined with 4.6 mg (0.021 mmol) PhIO; **11** with its side product was produced as the major species after 5 minutes, with a ^{1}H NMR identical to Method A.

Similar to **6**, regardless of preparation method, a side product would be present with nearly identical NMR shifts: ^{1}H NMR (300 MHz, CD_2Cl_2) δ 77.9, 77.1, 43.1, 38.6, 27.4, 23.7, 22.7, 16.1 (br), 9.2, 0.89, -1.3, -10.8 (br) ppm. This could be separated from **11** by stirring a solution of the mixture for 18 hours in MeCN and collecting the filtrate, or via MeCN/Et_2O vapor diffusion, where the mother liquor is collected upon precipitation of the side product. Attempts to identify this side product by XRD were unsuccessful.

*Synthesis of [LFe$_3$O(Pz)$_3$Fe(F)][OTf] (**12**). Method A.* 20.2 mg (0.014 mmol) **10** was dissolved in MeCN and froze in a liquid N_2-cooled cold well. This was combined with 6.8 mg (0.016 mmol) [Bu_4N][IO_4] in MeCN while thawing. The reaction became a brown suspension. After 16 hours, the solvents were removed under vacuum and the residue was washed with Et_2O,

toluene, THF, and eluted with MeCN to obtain 14.2 mg of a brown solid, corresponding to mostly clean (>90%) **12** (~70% yield). ^{1}H NMR (300 MHz, CD_2Cl_2) δ 127.7 (br), 77.3 (br), 74.5, 73.9, 59.9, 49.0, 31.1, 28.6, 23.4, 14.4,13.3, 11.4, 3.6 (br), -10.7 (br) ppm

Method B. 83.3 mg (0.058 mmol) **10** was dissolved in MeCN and froze in a liquid N_2-cooled cold well. This was combined with 370 μL of a tBuOOH solution (3.3 M in toluene diluted to 5% in MeCN; 0.061 mmol) and 7.1 mg (0.063 mmol) DABCO while thawing. The reaction became a brown suspension. After 12 hours, reaction was filtered.

Method C. 36.4 mg (0.024 mmol) of a suspension of **1** in MeCN was combined with 8.7 mg (0.033 mmol) $[Bu_4N][F]$ in MeCN to produce **12**.

*Synthesis of $LFe_3F(Pz)_3Fe(N_3)$ (**13**).* 20.9 mg (0.014 mmol) **10** in MeCN was mixed with 4.3 mg (0.015 mmol) $[Bu_4N][N_3]$ to produce an orange precipitate. After 2 hours, the precipitate was collected over a frit with celite, washed with minimal MeCN, eluted with CH_2Cl_2, and dried under vacuum to obtain 14.1 mg **13** as a red orange solid (75% yield). ^{1}H NMR (300 MHz, CD_2Cl_2) δ 111.2 (br), 75.9, 71.5, 41.1, 31.5, 30.8, 29.3, 15.0, 14.2, 11.1, 3.6, -2.5 (br), -18.9 (br) ppm

ELECTROCHEMICAL DETAILS

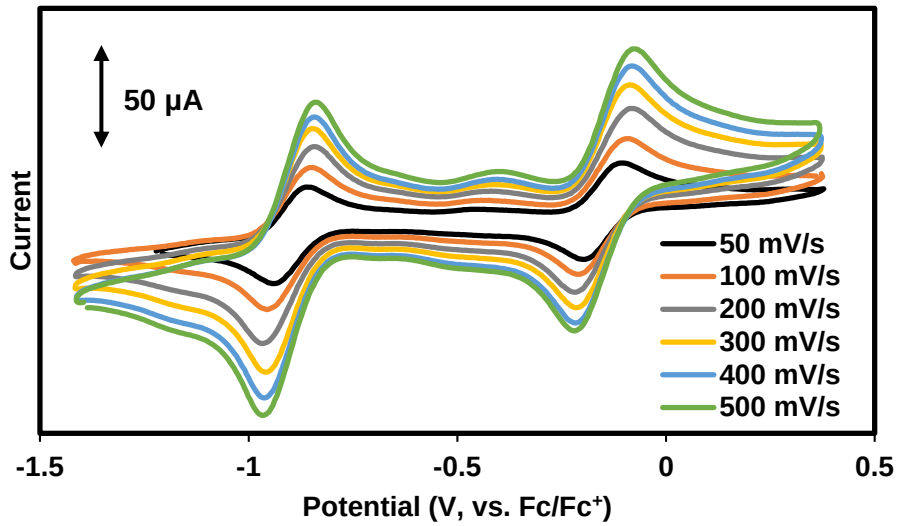

Figure 11. Cyclic voltammograms of $[LFe_3O(Pz)_3Fe][OTf]_2$ (**2**, 2 mM) in MeCN with 100 mM $[Bu_4N][PF_6]$ at various scan rates with glassy carbon, Pt-wire, and Ag-wire as working, counter, and reference electrode, respectively.

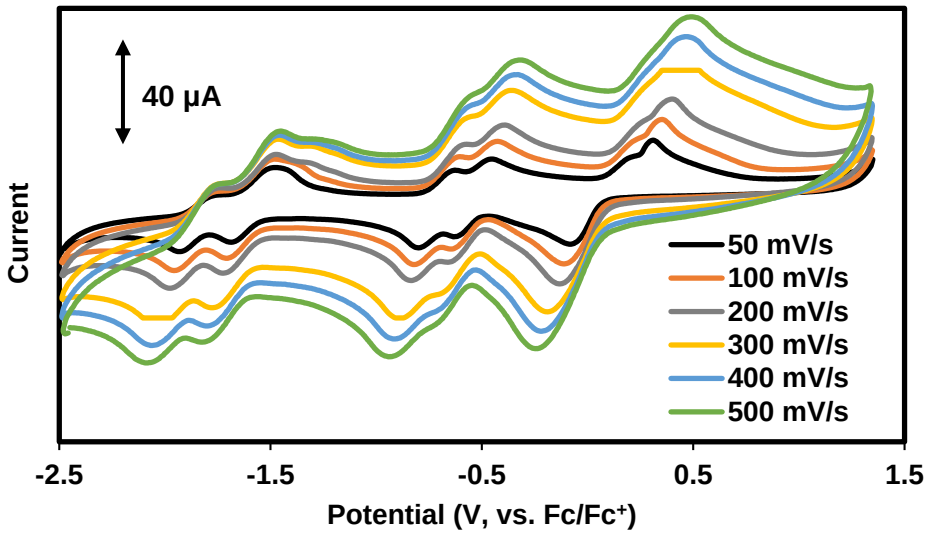

Figure 12. Cyclic voltammograms of $[(LFe_3O(Pz)_3Fe)_2O][OTf]_4$ (**6**, 2 mM) in CH_2Cl_2 with 100 mM $[Bu_4N][PF_6]$ at various scan rates with glassy carbon, Pt-wire, and Ag-wire as working, counter, and reference electrode, respectively.

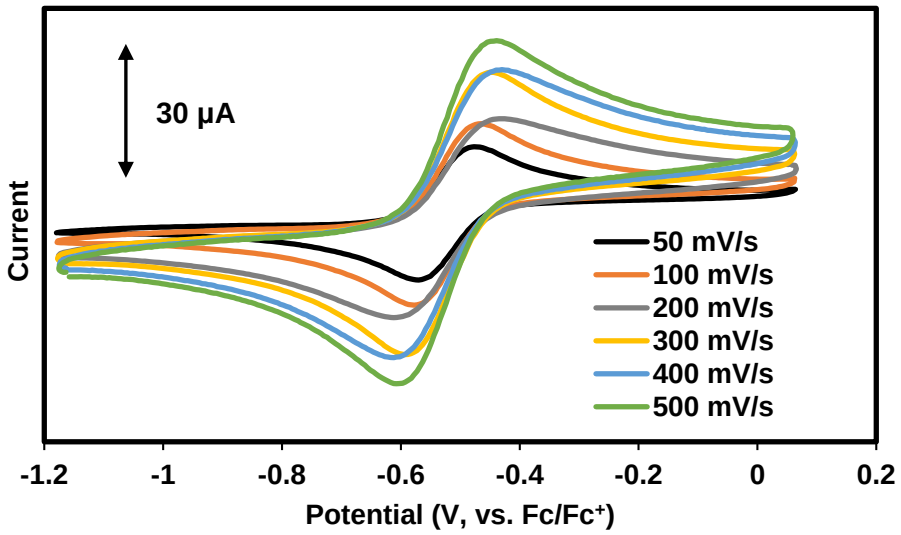

Figure 13. Cyclic voltammograms of $[LFe_3F(Pz)_3Fe][OTf]$ (**10**, 2 mM) in MeCN with 100 mM $[Bu_4N][PF_6]$ at various scan rates with glassy carbon, Pt-wire, and Ag-wire as working, counter, and reference electrode, respectively.

CRYSTALOGRAPHIC DETAILS

Crystal and refinement data for complexes 1 – 3-MeCN, 4, 6 – 11, and 13

	1[a]	2	3-MeCN	4	6
Empirical formula	$C_{78}F_2Fe_4N_{13}O_8$	$C_{95.28}H_{74.56}BCl_{8.56}F_3Fe_4N_{12}O_7S$	$C_{73}H_{52}F_3Fe_4N_{15}O_7S$	$C_{71.75}H_{49.5}ClF_{8.34}Fe_4N_{10.5}O_{12.61}S_3$	$C_{141.57}H_{102.25}Cl_{1.79}F_{12}Fe_8N_{24}O_{28.11}S_4$
Formula weight (g/mol)	1594.6	2124.57	1445.63	1717.62	3273.34
Radiation	CuKα (λ = 1.54178)	MoKα (λ = 0.71073)	CuKα (λ = 1.54178)	CuKα (λ = 1.54178)	CuKα (λ = 1.54178)
a (Å)	14.5023(10)	13.5663(9)	14.6522(6)	15.0846(9)	27.057(2)
b (Å)	19.6777(15)	17.3765(12)	19.7336(8)	15.0846(9)	14.2472(9)
c (Å)	47.912(4)	20.9073(14)	47.0533(17)	57.491(4)	40.302(3)
α (°)	90	84.592(3)	90	90	90
β (°)	93.256(3)	71.407(3)	91.934(2)	90	105.371(3)
γ (°)	90	80.890(2)	90	120	90
V (Å^3)	13650.8(18)	4607.4(5)	13597.3(9)	11329.2(15)	14980.0(18)
Z	8	2	8	6	4
Cryst. syst.	monoclinic	triclinic	monoclinic	trigonal	monoclinic
Space group	C2/c	P-1	C2/c	$P3_1$	C2/c
ϱ_{calc}g (cm^3)	1.552	1.531	1.412	1.511	1.451
2 Θ range (°)	7.392 to 69.236	4.656 to 56.496	7.518 to 158.694	4.61 to 158.116	6.776 to 149.24
μ (mm^{-1})	4.997	0.937	7.573	7.400	7.521
GOF	1.673	1.066	1.151	1.010	1.050
R1, wR2 (I>2σ (I))	R1 = 0.1227, wR2 = 0.3416	R_1 = 0.0694, wR_2 = 0.1905	R_1 = 0.1808, wR_2 = 0.3527	R_1 = 0.0674, wR_2 = 0.1620	R_1 = 0.1030, wR_2 = 0.2767

[a]Preliminary structure

	7[a]	**8**[a]	**9**	**10**	**11**	**13**[a]
Empirical formula	$C_{91}F_3Fe_4N_{13}O_9S$	$C_{80}Cl_{0.14}F_7Fe_4N_{12.36}O_7$	$C_{81}H_{55}Fe_4N_{13}O_9S_2$	$C_{68}H_{51}Cl_{1.91}F_4Fe_4N_{12}O_6S$	$C_{134}H_{94}F_8Fe_8N_{24}O_{13}S_2$	$C_{74.5}H_{47}FFe_4N_{18.39}O_3$
Formula weight (g/mol)	1873.11	1598.15	1641.90	1531.3	2884.12	1315.48
Radiation	MoKα (λ = 0.71073)	CuKα (λ = 1.54178)	CuKα (λ = 1.54178)	CuKα (λ = 1.54178)	MoKα (λ = 0.71073)	CuKα (λ = 1.54178)
a (Å)	18.1272(9)	19.0607(9)	55.590(10)	12.1433(15)	23.1614(12)	45.024(3)
b (Å)	16.5232(7)	15.6115(10)	12.4282(12)	23.562(4)	16.6931(8)	12.4123(7)
c (Å)	30.3724(15)	47.591(3)	22.632(2)	23.005(3)	33.0662(17)	51.116(3)
α (°)	90	90	90	90	90	90
β (°)	103.749(2)	91.952(2)	98.040(7)	99.807(5)	94.436(3)	109.157(5)
γ (°)	90	90	90	90	90	90
V (Å^3)	8836.5(7)	14153.3(14)	15482(3)	6485.8(16)	12746.3(11)	26984(3)
Z	4	8	8	4	4	16
Cryst. syst.	monoclinic	monoclinic	monoclinic	monoclinic	monoclinic	monoclinic
Space group	$P2_1/n$	C2/c	C2/c	$P2_1/C$	C2/c	C2/c
$\varrho_{calc}g$ (cm^3)	1.408	1.500	1.409	1.568	1.503	1.295
2 Θ range (°)	4.7 to 60.842	7.32 to 127.554	7.292 to 116.164	5.41 to 130.452	3.306 to 60.97	4.156 to 129.078
μ (mm^{-1})	0.739	7.504	6.937	8.690	1.003	7.231
GOF	1.517	1.620	1.115	1.042	1.119	1.032
R1, wR2 (I>2σ (I))	R_1 = 0.1346, wR_2 = 0.3671	R1 = 0.1532, wR2 = 0.4118	R_1 = 0.1353, wR_2 = 0.3364	R_1 = 0.0801, wR_2 = 0.163	R_1 = 0.0891, wR_2 = 0.2464	R_1 = 0.0945, wR_2 = 0.2274

[a]Preliminary structure

Special refinement details for [$LFe_3O(Pz)_3Fe(OAc)$][OTf] (1). This is a preliminary structure; 80% complete dataset. The counterions and solvent molecules were not modeled beyond the XT structure solution. The cluster was kept isotropic.

Special refinement details for [$LFe_3O(Pz)_3Fe$][OTf][BPh_4] (2). This structure contains five co-crystalized CH_2Cl_2 molecules. One was modeled as partially occupied (28%; C014 and Cl1 and Cl12). Another was positionally disordered, with a common carbon atom (Cl4 and Cl5, 21%, and Cl2 and Cl3, 79%). Relatively high residual Q peak density near the bound triflate, corresponding to a small amount of disorder for this ligand, was present, but could not be modeled adequately.

Special refinement details for [$LFe_3O(Pz)_3Fe(MeCN)$][OTf] (3-MeCN). The outersphere triflate is disordered over two positions, which is on a symmetry element. Each half triflate was modeled as partially occupied (fixed to 50%) with the CF_3 and SO_3 groups refined via EXYZ constraints. There were 1 or 2 co-crystalized solvent molecules, which could not be adequately modeled, and were left as isotropic C atoms.

Special refinement details for [$LFe_3O(Pz)_3Fe$][OTf]$_3$ (4). There are two clusters in the asymmetric unit. All but two of the six triflates are disordered; the disordered triflates bound to the clusters could not be completely modeled, but the sulfur and carbon of the minor component were modeled isotropically. The two outersphere triflates are positionally disordered with occupancies of 64% (S11 through O141) and 36% (S3CA through O142), and 60% (S0AA through O2AA) and 40% (S7CA through O21).

Special refinement details for [($LFe_3O(Pz)_3Fe)_2O$][OTf]$_4$ (6). There was a significant amount of solvent disorder in the crystal. It could be adequately modeled with CH_2Cl_2, Et_2O, and H_2O molecules. They were all modeled as partially occupied: Et_2O, 45%; CH_2Cl_2, 45%; H_2O, 55% (O18, O3AA) and 87% (O15).

Special refinement details for [$LFe_3O(Pz)_3Fe$(2-phenyl-anilide)][OTf] (7). This is a preliminary structure with a 37% complete dataset. The outersphere triflate was modeled, along with two co-crystalized THF molecules. There was some remaining solvent that could not be adequately modeled. Everything was modeled isotropically.

Special refinement details for [$LFe_3O(Pz)_3Fe$(3,5-trifluoromethyl-anilide)][OTf] (8). This is a preliminary structure with a 77% complete dataset. Everything was modeled isotropically. A complete triflate counterion and the trifluoromethyl groups could not be modeled adequately.

Special refinement details for [$LFe_3O(Pz)_3Fe$(para-toluenesulfonamide)][OTf] (9). Everything but the cluster was modeled isotropically, where no complete solvent molecule or counterion could be modeled.

Special refinement details for [$LFe_3F(Pz)_3Fe$][OTf] (10). The crystal contained a disordered co-crystalized CH_2Cl_2 molecule, with partial occupancies of 48% (C3, Cl2, and Cl6) and 52% (C3A, Cl1, and Cl3). 89% complete dataset.

Special refinement details for [$(LFe_3F(Pz)_3Fe)_2O$][OTf]$_2$ (11). The outersphere triflate was disordered over two positions in a ~50/50 ratio; however, each molecule could not be modeled completely. The presence of co-crystalized solvent molecules was suggested by large residual Q peaks, but nothing could be modeled adequately.

Special refinement details for $LFe_3F(Pz)_3Fe(N_3)$ (13). This is a preliminary structure with a 71% complete dataset. Everything was left isotropic. A number of co-crystallized MeCN molecules could be modeled.

References

1. Bertini, I.; Gray, H. B.; Stiefel, E. I.; Valentine, J. S. *Biological Inorganic Chemistry: Structure and Reactivity*. 1st ed.; University Science Books: Sausolito, California, 2007.
2. (a) Rittle, J.; Peters, J. C. *Proc. Natl. Acad. Sci.* **2013,** *110*, 15898-15903; (b) Taguchi, T.; Stone, K. L.; Gupta, R.; Kaiser-Lassalle, B.; Yano, J.; Hendrich, M. P.; Borovik, A. S. *Chemical Science* **2014,** *5*, 3064-3071; (c) Čorić, I.; Mercado, B. Q.; Bill, E.; Vinyard, D. J.; Holland, P. L. *Nature* **2015,** *526*, 96.
3. Li, F.; Meyer, R. L.; Carpenter, S. H.; VanGelder, L. E.; Nichols, A. W.; Machan, C. W.; Neidig, M. L.; Matson, E. M. *Chemical Science* **2018,** *9*, 6379-6389.
4. (a) Yu, F.; Pecoraro, V. L. *Polyhedron* **2013,** *64*, 99-105; (b) Xue, G.; De Hont, R.; Münck, E.; Que, L., Jr. *Nature Chemistry* **2010,** *2*, 400-405; (c) Caudle, M. T.; Pecoraro, V. L. *J. Am. Chem. Soc.* **1997,** *119*, 3415-3416; (d) Creutz, S. E.; Peters, J. C. *J. Am. Chem. Soc.* **2015,** *137*, 7310-7313; (e) Rittle, J.; McCrory, C. C. L.; Peters, J. C. *J. Am. Chem. Soc.* **2014,** *136*, 13853-13862.
5. Tsui, E. Y.; Kanady, J. S.; Day, M. W.; Agapie, T. *Chem. Commun.* **2011,** *47*, 4189-4191.
6. (a) de Ruiter, G.; Thompson, N. B.; Lionetti, D.; Agapie, T. *J. Am. Chem. Soc.* **2015,** *137*, 14094-14106; (b) Carsch, K. M.; de Ruiter, G.; Agapie, T. *Inorg. Chem.* **2017,** *56*, 9044-9054; (c) Arnett, C. H.; Chalkley, M. J.; Agapie, T. *J. Am. Chem. Soc.* **2018,** *140*, 5569-5578; (d) Reed, C. J.; Agapie, T. *Inorg. Chem.* **2017,** *56*, 13360-13367; (e) Reed, C. J.; Agapie, T. *J. Am. Chem. Soc.* **2018,** *140*, 10900-10908.
7. (a) Siegbahn, P. E. M. *BBA - Bioenergetics* **2013,** *1827*, 1003-1019; (b) Vinyard, D. J.; Brudvig, G. W. *Annu. Rev. Phys. Chem.* **2017,** *68*, 101-116; (c) Sproviero, E. M.; Gascón, J. A.; McEvoy, J. P.; Brudvig, G. W.; Batista, V. S. *J. Am. Chem. Soc.* **2008,** *130*, 3428-3442.
8. Hoffman, B. M.; Lukoyanov, D.; Yang, Z.-Y.; Dean, D. R.; Seefeldt, L. C. *Chem. Rev.* **2014,** *114*, 4041-4062.
9. (a) McDonald, A. R.; Que Jr, L. *Coord. Chem. Rev.* **2013,** *257*, 414-428; (b) Berry, J. F. *Comments Inorg. Chem.* **2009,** *30*, 28-66; (c) Lu, X.; Li, X.-X.; Seo, M. S.; Lee, Y.-M.; Clémancey, M.; Maldivi, P.; Latour, J.-M.; Sarangi, R.; Fukuzumi, S.; Nam, W. *J. Am. Chem. Soc.* **2019,** *141*, 80-83; (d) Wilding, M. J. T.; Iovan, D. A.; Wrobel, A. T.; Lukens, J. T.; MacMillan, S. N.; Lancaster, K. M.; Betley, T. A. *J. Am. Chem. Soc.* **2017,** *139*, 14757-14766.
10. (a) Vaddypally, S.; Kondaveeti, S. K.; Karki, S.; Van Vliet, M. M.; Levis, R. J.; Zdilla, M. J. *J. Am. Chem. Soc.* **2017,** *139*, 4675-4681; (b) de Visser, S. P.; Kumar, D.; Neumann, R.; Shaik, S. *Angew. Chem. Int. Ed.* **2004,** *43*, 5661-5665; (c) Khenkin, A. M.; Kumar, D.; Shaik, S.; Neumann, R. *J. Am. Chem. Soc.* **2006,** *128*, 15451-15460.
11. (a) Ruiter, G. d.; Carsch, K. M.; Takase, M. K.; Agapie, T. *Chemistry – A European Journal* **2017,** *23*, 10744-10748; (b) de Ruiter, G.; Thompson, N. B.; Takase, M. K.; Agapie, T. *J. Am. Chem. Soc.* **2016,** *138*, 1486-1489; (c) de Ruiter, G.; Carsch, K. M.; Gul, S.; Chatterjee, R.; Thompson, N. B.; Takase, M. K.; Yano, J.; Agapie, T. *Angew. Chem. Int. Ed.* **2017,** *56*, 4772-4776.
12. Horak, K. T. The Design and Synthesis of Transition Metal Complexes Supported by Non-innocent Ligand Scaffolds for Small Molecule Activation. PhD dissertation, California Institute of Technology, Pasadena, California, 2016.
13. (a) Nam, W.; Choi, S. K.; Lim, M. H.; Rohde, J.-U.; Kim, I.; Kim, J.; Kim, C.; Que, J. L. *Angew. Chem. Int. Ed.* **2003,** *42*, 109-111; (b) Wang, B.; Lee, Y.-M.; Seo, M. S.; Nam, W. *Angew. Chem. Int. Ed.* **2015,** *54*, 11740-11744; (c) MacBeth, C. E.; Golombek, A. P.; Young, V. G.; Yang, C.; Kuczera, K.; Hendrich, M. P.; Borovik, A. S. *Science* **2000,** *289*, 938-941; (d) Wijeratne, G. B.; Corzine, B.; Day, V. W.; Jackson, T. A. *Inorg. Chem.* **2014,** *53*, 7622-7634.
14. (a) Mankad, N. P.; Müller, P.; Peters, J. C. *J. Am. Chem. Soc.* **2010,** *132*, 4083-4085; (b) Iovan, D. A.; Betley, T. A. *J. Am. Chem. Soc.* **2016,** *138*, 1983-1993; (c) Spasyuk, D. M.; Carpenter, S. H.; Kefalidis, C. E.; Piers, W. E.; Neidig, M. L.; Maron, L. *Chemical Science* **2016,** *7*, 5939-5944; (d) Sazama, G. T.; Betley, T. A. *Inorg. Chem.* **2014,** *53*, 269-281.
15. Huang, C.-Y.; Doyle, A. G. *J. Am. Chem. Soc.* **2012,** *134*, 9541-9544.
16. Sun, H.; DiMagno, S. G. *J. Am. Chem. Soc.* **2005,** *127*, 2050-2051.
17. Rauchfuss, T. B. Bio-Inspired Iron and Nickel Complexes. In *Inorg. Synth.*, John Wiley & Sons, Inc.: 2010; pp 129-147.

18. Macikenas, D.; Skrzypczak-Jankun, E.; Protasiewicz, J. D. *J. Am. Chem. Soc.* **1999,** *121*, 7164-7165.
19. Altimari, J. M.; Niranjan, B.; Risbridger, G. P.; Schweiker, S. S.; Lohning, A. E.; Henderson, L. C. *Biorg. Med. Chem.* **2014,** *22*, 2692-2706.
20. Herbert, D. E.; Lionetti, D.; Rittle, J.; Agapie, T. *J. Am. Chem. Soc.* **2013,** *135*, 19075-19078.
21. (a) Herold, S.; Lippard, S. J. *Inorg. Chem.* **1997,** *36*, 50-58; (b) Singh, A. K.; Jacob, W.; Boudalis, A. K.; Tuchagues, J.-P.; Mukherjee, R. *Eur. J. Inorg. Chem.* **2008,** *2008*, 2820-2829; (c) Sutradhar, M.; Carrella, L. M.; Rentschler, E. *Eur. J. Inorg. Chem.* **2012,** *2012*, 4273-4278; (d) Schünemann, V.; Hauke, P. Mössbauer Spectroscopy. In *Applications of Physical Methods to Inorganic and Bioinorganic Chemistry*, Scott, R. A.; Lukehart, C. M., Eds. John Wiley & Sons: West Sussex, England, 2007; pp 243-269.